Intercalibration of SSM/I and SSMIS for the CSU FCDR

CSU Technical Report

Mathew R. P. Sapiano and Wesley Berg

July 2013

http://rain.atmos.colostate.edu/FCDR/

TABLE of CONTENTS

1. INTRODUCTION 4

2. INTERCALIBRATION TECHNIQUES 4

2.1 Reanalysis Transfer 5
2.2 Polar Crossover 6
2.3 TMI Matchups 7
2.4 Vicarious Cold Calibration 7
2.5 Amazon Warm Calibration 8

3. COMBINATION OF TECHNIQUES 9

3.1 SSM/I Sensors 9
3.2 SSMIS Sensors 11

4. REFERENCES 12

LIST of FIGURES

Figure B-1. Plots of intercalibration differences from each implementation by channel for F08-F10. 18

Figure B-2. Plots of intercalibration differences from each implementation by channel for F10-F13. 19

Figure B-3. Plots of intercalibration differences from each implementation by channel for F11-F13. 20

Figure B-4. Plots of intercalibration differences from each implementation by channel for F13-F14. 21

Figure B-5. Plots of intercalibration differences from each implementation by channel for F13-F15. 22

Figure B-6. Plots of intercalibration differences from each implementation by channel for F13-F16. 23

Figure B-7. Plots of intercalibration differences from each implementation by channel for F13-F17. 24

Figure B-8. Plots of intercalibration differences from each implementation by channel for F17-F18. 25

LIST of TABLES

Table 1. Final Tb offsets in Kelvin versus F13 SSM/I (version January 2013). 10

Table 2: Standard deviation of Tb offsets in Kelvin from five techniques. (version January 2013) 10

Table 3. Mean intercalibration differences from each implementation for F08-F10 14

Table 4. Mean intercalibration differences from each implementation for F10-F11 14

Table 5. Mean intercalibration differences from each implementation for F11-F13 14

Table 6. Mean intercalibration differences from each implementation for F13-F14 15

Table 7. Mean intercalibration differences from each implementation for F13-F15 15

Table 8. Mean intercalibration differences from each implementation for F13-F16 16

Table 9. Mean intercalibration differences from each implementation for F13-F17 16

Table 10. Mean intercalibration differences from each implementation for F17-F18 17

ACRONYMS AND ABBREVIATIONS

Acronym or Abbreviation	Meaning
CATBD	Climate Algorithm Theoretical Basis Document
CDR	Climate Data Record
NCDC	National Climatic Data Center
NOAA	National Oceanic and Atmospheres Administration

1. Introduction

An important aspect in creating an FCDR is to remove discontinuities between sensors so as to remove the potential for erroneous trends. In the case of the SSM/I and SSMIS FCDR, the goal was to intercalibrate all sensors to a common standard using multiple approaches. Five distinct techniques have been applied including direct polar matchups, double differencing against model simulations from reanalysis profile data, double differencing against matchups with the TRMM Microwave Imager, vicarious cold calibration and an Amazon warm calibration. Multiple realizations of three of the five techniques have been applied using different reanalysis data and retrieval techniques to account for EIA dependent differences between sensors. It is important to note that intercalibration does not imply that the derived correction will completely homogenize observations from the sensor. Instead, the intercalibration procedure must ensure that measurements between the sensors are “physically” consistent. In addition to calibration errors, observations from the sensors can differ due to several physical mechanisms including diurnal sampling differences, channel differences and view angle or Earth Incidence Angle (EIA) differences. F13 was chosen as a calibration standard due to its longevity and its stable orbit. Although the SSMIS has 24 channels, the focus of this work was the SSM/I-like channels (19, 22, 37 and 91 GHz) and intercalibration of the other channels is neglected in the FCDR. The following summarizes the approach used for the FCDR and is based on the techniques described by Sapiano et al. (2012).

2. Intercalibration Techniques

Five different intercalibration techniques were applied to the SSM/I and SSMIS Tb. Three of these five techniques had several different implementations to give a total of 10 sets of realizations, not all of which are completely independent. The comparison of multiple intercalibration techniques allows for an assessment of the errors associated with the techniques and how sensitive the results are to the assumptions made. The bulk of the techniques cover the colder non-cloudy/non-rainy Tb, with only a single technique (Amazon Warm Calibration) at the warm end.

Each of the techniques uses a common methodology, although the assumptions and screening applied differ. Only one of the techniques employs direct comparisons between two sensors (polar matchups). The other techniques use a transfer standard that takes the form of either matchups with another satellite (TMI matchups), a numerical weather prediction model (reanalysis transfer), a fixed Earth point (Amazon warm calibration) or a theoretical value (vicarious cold calibration). In all cases, it is critical to account for differences in the Earth Incidence Angle (EIA) in order to obtain a physically consistent intercalibration. This is done using several methods, but each of these involves simulating brightness temperatures using the computed EIA for each sensor/pixel. The resulting simulated differences comprise the expected or physical component of the observed Tb difference resulting from differences in the viewing geometry between sensors. As such, they are subsequently subtracted from the total observed differences to obtain the residual difference in the sensor calibration. Each of the techniques also applies screening to ensure that only valid data (valid under the

assumptions for each technique) are used. Finally, since this intercalibration is to be used for a climate record, each of the techniques was applied over the longest possible period to maximize sampling and to facilitate studies into how the intercalibration changes over time, if at all.

2.1 Reanalysis Transfer

One of the drawbacks for techniques involving direct comparisons (i.e. polar crossovers) is that they do not provide estimates for all SSM/I satellites. In particular, the F08 data in the FCDR has no overlaps with other satellites and so direct matchups or matchups with another reference satellite are not possible. One of the ways to address this issue is to use a radiative transfer model to simulate Tb using reanalysis data from a global forecast model. The difference between the simulated and observed Tb can then be used to calculate a residual difference for each sensor. The difference between these sensor residuals is then used to estimate the calibration difference between sensors, with the reanalysis model essentially becoming the transfer standard.

There are several potential issues with this technique that require special care. One of the biggest issues is the propagation of model errors into the calibration after taking the difference between the residuals. The first way this can occur is if different periods are used to calculate the residuals, so that either time-dependent errors or errors related to weather variations are aliased into the results. In most cases this is addressed by using a common observing period for the two satellites, but that is not possible for F08. For F08, these issues can be greatly ameliorated by comparing F08 values with those from the first ~2 years of F10. This should minimize the effect of potential climate trends in reanalysis model data and provide enough sampling to remove weather effects. The second potential way that model errors can affect the intercalibration comes from comparing satellites observing at different times of day. If the model has errors associated with the diurnal cycle, these can propagate into the intercalibration and might be particularly large for a model with a six-hourly time step. This issue will be excplicitly dealt with by several of the techniques. Finally, there is a potential conflict in using the reanalysis data in that most models assimilate the SSM/I data. It could be argued that the models are therefore drawn towards the original (and presumably sub-optimal) calibration of the satellite. However, the assimilation of satellite data into the reanalysis system involves bias adjustment of the satellite data to be consistent with the model, which is in itself a recalibration to the underpinning in situ observations. Thus, the reanalysis models use the variability of the satellites but are not biased by them and so this problem is expected to be negligible.

In order to obtain coverage of the whole SSM/I record, reanalysis data from the National Aeronautics and Space Administration (NASA) Modern Era Reanalysis (MERRA; Reinecker et al., 2011) and from the European Center for Medium Range Weather Forecasting (ECMWF) Interim Reanalysis (ERA-I; Dee et al., 2011) were obtained. Data were averaged to a common one-degree spatial resolution with 25 vertical layers every three hours for MERRA and 29 vertical layers every six hours for ERA-I. The variables used in the radiative transfer model to construct the atmospheric profile included pressure, geopotential, temperature, humidity and liquid water as well as

surface wind speed, skin temperature and surface pressure and the EIA for the corresponding satellite data. The radiative transfer model is the same as that used by Elsaesser and Kummerow (2008). Tb were gridded to one-degree resolution and grid boxes containing the edge of scan were discarded so as to use only "full" grid boxes. An aggressive land mask was used to screen out land and near coast grid boxes and boxes outside 60° N/S were discarded to eliminate sea ice. In addition, the standard deviation of the 85 GHz Tb in the one-degree box was used to screen out clouds and rain by eliminating those with a value greater than three Kelvin. This threshold was chosen by trial-and-error to minimize contaminated pixels, whilst retaining enough sampling. It was also found to be necessary to screen for clouds and rain in the model profiles, so these were removed when total column liquid water exceeded ten grams per square meter. The model grid box closest in time to the observations was then selected and used to compute simulated Tb for comparison with observed Tb.

2.2 Polar Crossover

The SSM/I instruments were flown with the goal of having dual coverage with one sensor crossing the equator at around 6am/pm (descending/ascending) and another around 8am/pm. Since they were flown on the sun-synchronous polar orbiting DMSP, the only direct overlaps between SSM/I sensors occur near the poles. Direct polar matchups were not possible for F8 since that sensor did not significantly overlap in time with any of the others.

Coincident observations or crossovers between sensors were defined as those occurring within 30 minutes of each other. Two methods were tested for obtaining matched data. The first method involved matching individual pixels within 50km and 30 minutes. The second method involved gridding the data onto a roughly 100km equal-area global grid and then matching grid boxes. Similar results were found for each of the methods, but the second method provides a number of advantages. First, in order to account for differences in EIA between the two sensors, it was necessary to match one-degree reanalysis model data to the crossovers and the gridded data is more comparable to the reanalysis data than the pixel data. Second, the gridded data made it easier to screen out clouds by using the standard deviation of the 85GHz Tb within the grid-box. Last, it was considerably faster to process the grid averaged values.

Once the matchups were identified, a liberal land mask was used to screen out grid boxes over land as well as near the coast. Ice concentration from the "National Ice Center Arctic sea ice charts and climatologies in gridded format" dataset (National Ice Center, 2009) were used to identify grid boxes that were completely ice free (open ocean). Cloud free grid boxes where identified using the standard deviation of the 85v and 85h channels within each grid box, with only those boxes with a value less than three Kelvin being used. Profile data from MERRA were gridded to the same equal area grid and used to simulate Tb for each sensor based on the EIA. The difference between the simulated Tb for the two sensors was then subtracted from the difference between the observed Tb to obtain the intercalibration difference between those two sensors.

2.3 TMI Matchups

The TRMM Microwave Imager (TMI) has a very similar channel complement to SSM/I and due to its low inclination orbit, which samples the full diurnal cycle, it can be used as a transfer standard to eliminate the impact of diurnal cycle variability while providing direct matchups at low latitudes. While TMI is very similar in design to the SSM/I (TMI was based on the SSM/I design), it has a different view angle to SSM/I as well as some slight differences in channel frequencies, particularly the water vapor channel, which is at 21.3 GHz for TMI. Another drawback of this approach is that TRMM was launched in late 1997 meaning that data are not available for intercalibrating F08 and F10 and there are only ~2 years of overlap for F11.

As with the polar crossovers technique, ground-tracks for each satellite were used to identify crossovers between each of the SSM/I sensors and TMI. Tb were averaged onto a one-degree latitude/longitude grid, with grid-boxes containing the edge-of-scan discarded to obtain only "full" boxes. A land mask was used to remove land pixels (sea ice was not a problem since TRMM flies between 37.5° S/N) and the standard deviation of the 85 GHz Tb was used to remove rain/cloud scenes. For the SSM/I and TMI comparisons not only do differences in EIA need to be accounted for, but also the differences in channel frequencies.

In order to better understand potential errors in the simulated Tb associated with channel and EIA differences, three different techniques were used to estimate these differences. Note that all three of these approaches use the same radiative transfer model. The first technique involved the retrieval of geophysical parameters from TMI using the optimal estimation (OE) technique described in Elsaesser and Kummerow (2008). This OE technique is an iterative approach to inverting a radiative transfer model to obtain estimates of wind speed, total precipitable water and cloud liquid water that are consistent with the observed Tb and the specified sea surface temperature (SST; Reynolds et al., 2007). The retrieved geophysical variables were then used to simulate Tb for both TMI and SSM/I to account for differences in EIA and channel characteristics including frequency. The other two techniques used to account for EIA and channel differences are similar to the technique described for the reanalysis transfer intercalibration technique. The reanalysis surface and profile data from MERRA and ERA-I were used to simulate the expected Tb differences between TMI and SSM/I, providing two additional realizations of these differences based on reanalysis data.

2.4 Vicarious Cold Calibration

As previously mentioned, one of the challenges in intercalibrating the SSM/I record is connecting F08 to F10 and hence the rest of the series. Since there are no direct overlaps with any other radiometer, some other transfer standard must be used for F08. Tb simulated from reanalysis data have already been mentioned as a method that can

be used for this purpose, but another approach is to use the Vicarious Calibration method described by Ruf (2000). The approach exploits the property that the minimum Tb over the open ocean occurs at a fixed sea-surface temperature that varies by channel and EIA. The technique involves estimating the minimum Tb over the open ocean using a statistical approach. There are still several drawbacks to this approach, most importantly that the theoretical minimum Tb for the 85GHz channels occurs at a Tb that is not regularly observed over the open ocean. The technique instead provides an estimate of the observed statistical minimum for the 85 GHz channels.

Histograms of Tb for each channel were calculated from the overlap period for the two sensors to be compared. The Tb were screened to remove scenes with high values of atmospheric water vapor so that the histograms represent only the cold end of oceanic Tb. A polynomial fit was then used to estimate the minimum Tb from the histogram. The EIA dependence was removed by repeating the procedure using simulated Tb based on the OE, Merra and ERA-I profiles. The minimum can be distorted by changes in the water vapor distribution over time, so a common period of overlap was used to estimate the vicarious cold minimum. In the case of F08, there is no overlap with the other sensors and so two years of F08 data were compared to four different years of F10 data. Whilst not overlapping, the use of relatively short periods that are close in time should ameliorate the effect of any water vapor changes that would be expected to occur on longer timescales.

2.5 Amazon Warm Calibration

The techniques presented so far are limited to open-ocean, cloud/free Tb, which correspond to the colder part of the spectrum of observed Tb. It is desirable to have an estimate of the differences between the satellites over the warm part of the spectrum in order to determine if there is any slope (gain) in the intercalibration differences. The warmer Tb are predominantly observed over land due to the much higher surface emissivities. This complicates the radiative transfer modeling and can lead to larger errors and the techniques described so far are not sufficient for this purpose. For an estimate of the intercalibration at the warm end, we used the technique described by Brown and Ruf (2005), which is based on identifying a relatively large, near-blackbody target on Earth and using crossovers from each of the satellites to estimate intercalibration values. The target and methodology used in this study is the same as that used by Brown and Ruf (2005), who used a homogeneous area over the Amazon as the target. Once crossovers over the target area were obtained, a physical model described by Brown and Ruf (2005) was used to simulate Tb for each sensor so that the target area could be used as a transfer standard. The error of the physical model was estimated by Brown and Ruf (2005) as 0.57K.

One of the major issues with the application of this technique to the SSM/I record is the effect of the diurnal cycle, which is relatively large over land. As shown in fig 1a the SSM/I sensors rarely observed the same time of day. In addition, satellite orbit drift leads to changes in the observing time that could result in trends in the intercalibration that are aliased with the diurnal sampling. In order to remove any diurnal effect, the comparisons were done using TMI as a transfer standard since its orbit provides

samples throughout the day. Matchups with SSM/I and TMI over the target area were used to estimate the intercalibration for the SSM/I relative to the TMI. These matchups were therefore obtained only for F13, F14 and F15 since they have long overlaps with TMI. The SSM/I – TMI comparisons were then used to estimate the intercalibration values between each combination of F13, F14 and F15. The original technique was extended for use with the SSM/I high frequency channels by extrapolating the linear dependence of the single scatter albedo on frequency used in the original Brown and Ruf (2005) formulation to 85 GHz. This extrapolation is justified by the emissivity retrievals of Prigent et al. (2008) using SSM/I data over dense vegetation. As was done by Brown and Ruf (2005), only 85 GHz data for which the v, h difference was less than 3 Kelvin were used to select de-polarized, near-blackbody regions. This also filters out cloud and rain contaminated data as described above in Section 3A. To ensure the quality of the resulting Amazon reference parameters, only retrievals for which the root mean squared fitting error was less than 1.5 Kelvin were used. At this threshold, 95% of the data that met the 3-Kelvin v/h difference requirement remain.

3. Combination of techniques

3.1 SSM/I Sensors

Appendix A shows the results from all five techniques (where applicable) with multiple implementations for several of the techniques based on different geophysical parameters including retrieved values from the OE as well as from MERRA and ERA-I reanalysis. Results are shown for each channel and for each combination of satellites used for intercalibration. All satellites are intercalibrated to F13 in the FCDR. F10, F11, F14, and F15 all have sufficient overlap with F13 that direct comparison was possible. Intercalibration for F08 was calculated via F10 to F11 to F13. Initially, the results from the different implementations were first averaged to obtain a single set of values as a function of Tb from each of the five techniques and then the mean of the five techniques was used to estimate the mean intercalibration to be used in the FCDR creation. Validation of this result based on geophysical retrievals of both non-precipitating ocean scenes using the optimal estimation algorithm (Elsaesser and Kummerow, 2008) and precipitation over oceans based on the latest operational GPROF retrieval algorithm (Kummerow et al. 2001, 2011), however, showed larger than acceptable differences. As a result, the decision was made to revert to the TMI matchup results using geophysical parameters from ERA-I reanalysis to compute the simulated differences between sensors. The double difference approach used in the TMI matchup technique uses coincident observations and most of the radiative transfer model errors cancel given the similarity of the channel characteristics. For the SSM/I sensors the frequencies, spatial resolution etc. are identical, thus only the small differences in EIA or view angles must be accounted for by the model-simulated difference. Because of these factors, the TMI matchup technique has smaller overall errors so the final Tb offsets for F11, F14, and F15 were based only on this technique. Since TMI was launched after F08 and F10 died no coincident overpasses are available for those sensors and thus the combination approach described above was used. As a result, the residual calibration errors for F08 and F10 are expected to be larger than for the other SSM/I sensors. Subsequent

validation of the FCDR Tb data based on the non-precipitating and precipitation retrievals over ocean subsequently show much better agreement between the F11, F13, F14, and F15 sensors.

For the SSM/I sensors, the Amazon warm calibration technique provided an assessment of whether a scene temperature dependent Tb offset was required. Given that the error on the Amazon warm calibration results was calculated as 0.57K, however, there was insufficient evidence that a scene temperature dependent correction was warranted. In keeping with a philosophy to make things as simple as possible unless otherwise warranted, the decision was made to apply a simple Tb offset to intercalibrate the SSM/I sensors to F13.

The final Tb offsets used to intercalibrate the SSM/I sensors to F13 are given in Table 1 and the standard deviations of the five techniques are given in Table 2. The values for F14 and F15 are relatively small, which reflects the fact that these sensors were fabricated at the same time as F13. The earlier sensors tend to require larger intercalibration offsets that perhaps reflect modifications in the latter sensors through the ongoing SSM/I calibration/validation process. F08 in particular requires offsets larger than 1K for three of the channels, but even these offsets are relatively small due to the common design of the sensors. As noted above, the uncertainties for the F08 and F10 sensors are also larger due to the lack of an overlap period with F13 as well as reliance on intercalibration approaches such as reanalysis transfer and polar crossovers that have larger uncertainties than the TMI matchup double difference approach.

	19V	19H	22V	37V	37H	85/91V	85/91H
F08	0.65	0.16	1.42	0.82	1.64	1.91	-0.52
F10	0.05	0.16	1.27	-0.21	0.48	0.37	0.11
F11	0.32	-0.02	0.38	0.78	0.46	-0.64	-1.46
F13	0.00	0.00	0.00	0.00	0.00	0.00	0.00
F14	0.21	0.29	0.18	-0.47	0.14	0.00	0.18
F15	0.79	0.11	0.35	0.01	0.22	0.47	0.34

Table 1. Final Tb offsets in Kelvin versus F13 SSM/I (version January 2013).

	19V	19H	22V	37V	37H	85/91V	85/91H
F08	0.05	0.04	0.07	0.03	0.05	0.41	0.20
F10	0.03	0.04	0.09	0.01	0.04	0.07	0.13
F11	0.01	0.03	0.05	0.02	0.02	0.05	0.11
F13	0.00	0.00	0.00	0.00	0.00	0.00	0.00
F14	0.11	0.05	0.08	0.05	0.07	0.04	0.04
F15	0.09	0.02	0.07	0.05	0.03	0.07	0.04

Table 2: Standard deviation of Tb offsets in Kelvin from five techniques. (version January 2013)

3.2 SSMIS Sensors

Originally, the same intercalibration techniques were applied to the SSMIS sensors on board DMSP F16, F17, and F18. The resulting calibration differences for the various techniques are shown in Figures D-6, D-7, and D-8, and the mean offsets are given in Tables 8, 9, and 10. Differences between SSM/I and SSMIS are larger for several of the channels compared to those between the SSM/I sensors, which reflects the fact that these are different sensor designs. Differences are smaller for lower frequencies with offsets against F13 in the range of 0.5 to 1K. Differences 1 to 3K are observed at 37 GHz. For the comparison of 85V and 91V, differences between F13 and F16 are smaller than those for F13 versus F17 and F18. In addition, the variability among the various techniques is also significantly larger.

Unfortunately, the application of the resulting Tb to geophysical retrieval algorithms based on the simple mean calibration offset, as done with the SSM/I sensors, revealed substantial differences in both non-precipitating and precipitating ocean scenes. Further investigation revealed several issues that were not a significant factor for the SSM/I sensors. One issue was the existence of large calibration differences between ascending and descending passes, indicating calibration biases associated with heating/cooling of the spacecraft/sensor. A second issue involved significant variations in the calibration differences as a function of the scene temperature. To address these issues, the TMI double difference approach was used to develop a correction to the Tb based on the angle of the sun relative to the spacecraft. Further details on the development and application of this sun-angle correction are given in the technical report by Berg and Sapiano (2013). Because the sun-angle correction uses double differences with TMI, it also has the effect of removing intercalibration biases relative to TMI. The final intercalibration to F13, therefore, is a scene-temperature dependent correction to adjust the Tb from the TMI calibration to F13. Unlike the simple offsets used for the SSM/I sensors, the final SSMIS intercalibration uses a series of tie points, or Tb offsets at specified scene temperature values based on the TMI double difference analysis. Observed Tb values in between these tie points are linearly interpolated from the adjacent tie point intercalibration values. Observed Tb values outside the range of specified tie point values simply use the Tb offset corresponding to the nearest tie point temperature. This means no extrapolation of the intercalibration offsets is done outside the range of available tie points. Since the TMI double difference approach uses non-precipitating ocean scenes, which correspond to the colder end of the observed Tb range, potential issues may remain regarding changes in the intercalibration biases over warmer scenes such as land where the surface emissivity is much higher.

4. References

Berg, W. and M. R. P. Sapiano, 2013: Corrections and APC for SSMIS, Technical report, Colorado State University, http://rain.atmos.colostate.edu/FCDR.

Brown, S. and C. Ruf, "Determination of a Hot Blackbody Reference Target over the Amazon Rainforest for the On-orbit Calibration of Microwave Radiometers," *J. Oceanic Atmos. Tech.*, vol. 22, no. 9, pp. 1340-1352, Sep. 2005.

Dee, D. P., S. M. Uppala, A. J. Simmons, P. Berrisford, P. Poli, S. Kobayashi, U. Andrae, M. A. Balmaseda, G. Balsamo, P. Bauer, P. Bechtold, A. C. M. Beljaars, L. van de Berg, J. Bidlot, N. Bormann, C. Delsol, R. Dragani, M. Fuentes, A. J. Geer, L. Haimberger, S. B. Healy, H. Hersbach, E. V. Hólm, L. Isaksen, P. Kållberg, M. Köhler, M. Matricardi, A. P. McNally, B.M. Monge-Sanz, J.-J. Morcrette, B.-K. Park, C. Peubey, P. de Rosnay, C. Tavolato, J.-N. Thépaut, and F. Vitart, “The ERA-Interim reanalysis: configuration and performance of the data assimilation system,” *Quarterly Journal of the Royal Meteorological Society*, vol. 137, pp.553–597, Apr 2011.

Elsaesser, G. S. and C. K. Kummerow, "Towards a fully parametric retrieval of the non-raining parameters over the global oceans," *J. Appl. Meteor. & Climatol.*, vol. 47, pp. 1599–1618, Jun. 2008.

Kummerow, C. D., S. Ringerud, S. Crook, D. Randel, and W. Berg, 2011: An observationally generated a-priori database for microwave rainfall retrievals, *J. Atmos. Oceanic Technol.,* 28, 113-130.

Kummerow, C. D. and Coauthors, 2001: The Evolution of the Goddard Profiling Algorithm (GPROF) for rainfall estimation from passive microwave sensors. *J. Appl. Meteor*., 40, 1801–1820.

National Ice Center, “*National Ice Center Arctic sea ice charts and climatologies in gridded format,*” Edited and compiled by F. Fetterer and C. Fowler. Boulder, Colorado USA: National Snow and Ice Data Center. Digital media. 2009.

Prigent, C., E. Jaumouillé, F. Chevallier, F. Aires, “A Parameterization of the Microwave Land Surface Emissivity between 19 and 100 GHz, Anchored to Satellite-Derived Estimates,” *IEEE Trans. Geosci. Remote Sens.*,vol. 466, no. 2, pp. 344-352, Feb. 2008.

Reynolds, R. W., T. M. Smith, C. Liu, D. B. Chelton, K. S. Casey, and M. G. Schlax, “Daily high-resolution blended analyses for sea surface temperature,” *J. Climate*, vol. 20, pp. 5473-5496, Nov. 2007.

Rienecker, M. M., M.J. Suarez, R. Gelaro, R. Todling, J. Bacmeister, E. Liu, M.G. Bosilovich, S.D. Schubert, L. Takacs, G.-K. Kim, S. Bloom, J. Chen, D. Collins, A. Conaty, A. da Silva, W. Gu, J. Joiner, R. D. Koster, R. Lucchesi, A. Molod, T. Owens, S. Pawson, P. Pegion, C. R. Redder, R. Reichle, F. R. Robertson, A. G. Ruddick, M. Sienkiewicz, J. Woollen, “MERRA - NASA's Modern-Era Retrospective Analysis for Research and Applications**,”** *J. Climate*, vol. 24, pp. 3624-3648, Jul 2011.

Ruf, C. S., "Detection of calibration drifts in spaceborne microwave radiometers using a vicarious cold reference," *IEEE Trans. Geosci. Remote Sens.*, vol. 38, num. 1, 44-52, Jan 2000.

Sapiano, M. R. P., Berg, W. K., McKague, D. S., and Kummerow, C. D., 2013: Towards an Intercalibrated Fundamental Climate Data Record of the SSM/I Sensors, *IEEE Trans. Geosci. Remote Sens.*, 51, 1492-1503.

Appendix A: Results from individual techniques

Method	19V	19H	22V	37V	37H	85V	85H
Merra Simulation	-0.66	-0.03	-0.38	-0.89	-0.93	-0.69	0.45
ERA-I Simulation	-0.73	-0.09	-0.27	-1.05	-1.19	-0.81	0.20
VCC (OE)	-0.40	0.06	0.02	-0.99	-1.10	-2.28	0.87
VCC (Merra)	-0.64	-0.04	-0.34	-1.21	-1.39	-2.34	0.91
VCC (ERA-I)	-0.50	0.12	-0.27	-1.05	-1.20	-2.42	1.17
Mean Beta Mean	-0.60	-0.01	-0.26	-1.03	-1.15	-1.55	0.65
Beta Cal SD	0.09	0.05	0.06	0.06	0.08	0.80	0.33

Table 3. Mean intercalibration differences from each implementation for F08-F10

Method	19V	19H	22V	37V	37H	85V	85H
Polar Crossover	0.10	-0.20	-1.25	0.83	-0.03	-1.08	-1.40
Merra Simulation	-0.41	-0.55	-1.99	0.44	-0.43	-1.56	-1.93
ERA-I Simulation	-0.11	0.16	-1.59	0.63	0.16	-1.23	-1.45
VCC (OE)	0.37	0.07	-0.10	0.98	0.16	-0.40	0.28
VCC (Merra)	0.24	-0.34	-1.04	1.07	-0.16	-0.67	-0.76
VCC (ERA-I)	0.27	-0.39	-0.92	0.95	-0.17	-0.69	-0.67
Mean Beta Mean	0.05	-0.20	-1.24	0.79	-0.07	-1.02	-1.16
Beta Cal SD	0.23	0.01	0.45	0.19	0.05	0.33	0.56

Table 4. Mean intercalibration differences from each implementation for F10-F11

Method	19V	19H	22V	37V	37H	85V	85H
Polar Crossover	-0.15	0.14	-0.21	-0.65	-0.41	0.55	1.23
Merra Simulation	-0.14	0.26	-0.05	-0.67	-0.35	0.76	1.66
ERA-I Simulation	-0.24	0.24	-0.02	-0.67	-0.24	0.67	1.54
TMI match (OE)	-0.23	0.13	-0.26	-0.71	-0.38	0.65	1.53
TMI match (Merra)	-0.23	0.12	-0.26	-0.71	-0.41	0.67	1.52
TMI match (ERA-I)	-0.21	0.13	-0.28	-0.71	-0.38	0.63	1.40
VCC (OE)	-0.10	0.17	-0.03	-0.75	-0.32	0.40	0.80
VCC (Merra)	-0.26	0.07	-0.35	-0.80	-0.42	0.26	0.66
VCC (ERA-I)	-0.30	-0.06	-0.42	-0.73	-0.52	0.23	0.37
Mean Beta Mean	-0.19	0.14	-0.19	-0.70	-0.38	0.55	1.23
Beta Cal SD	0.03	0.07	0.09	0.04	0.05	0.16	0.38

Table 5. Mean intercalibration differences from each implementation for F11-F13

Method	19V	19H	22V	37V	37H	85V	85H
Polar Crossover	0.18	0.20	0.29	-0.41	0.11	0.27	0.44
Merra Simulation	0.07	0.21	0.13	-0.49	0.17	0.05	0.26
ERA-I Simulation	0.15	0.23	0.29	-0.35	0.21	0.10	0.34
TMI match (OE)	0.18	0.27	0.17	-0.46	0.11	0.05	0.22
TMI match (Merra)	0.19	0.27	0.18	-0.46	0.12	0.04	0.22
TMI match (ERA-I)	0.21	0.29	0.18	-0.47	0.14	0.00	0.18
VCC (OE)	-0.02	-0.16	0.04	-0.60	-0.04	0.06	-0.14
VCC (Merra)	0.08	0.08	0.19	-0.46	0.18	0.01	-0.01
VCC (ERA-I)	0.12	0.06	0.26	-0.54	0.23	0.09	0.08
Amazon Warm Cal	-0.16	-0.14	0.15	-0.40	-0.42	0.43	0.44
Mean Beta Mean	0.13	0.17	0.21	-0.46	0.14	0.11	0.24
Beta Cal SD	0.05	0.10	0.05	0.05	0.03	0.09	0.17

Table 6. Mean intercalibration differences from each implementation for F13-F14

Method	19V	19H	22V	37V	37H	85V	85H
Polar Crossover	0.57	-0.19	0.26	-0.06	0.15	0.71	0.56
Merra Simulation	0.60	-0.01	0.24	-0.12	0.21	0.51	0.47
ERA-I Simulation	0.53	-0.01	0.28	-0.09	0.22	0.46	0.47
TMI match (OE)	0.78	0.08	0.33	0.02	0.20	0.56	0.42
TMI match (Merra)	0.78	0.08	0.33	0.01	0.20	0.56	0.42
TMI match (ERA-I)	0.79	0.11	0.35	0.01	0.22	0.47	0.34
VCC (OE)	0.53	-0.27	0.02	-0.23	0.19	0.39	0.09
VCC (Merra)	0.40	-0.20	0.08	-0.26	0.02	0.34	0.04
VCC (ERA-I)	0.50	-0.31	0.17	-0.27	0.11	0.28	0.06
Amazon Warm Cal	-0.65	-0.61	-0.62	-0.62	-0.65	0.16	0.22
Mean Beta Mean	0.60	-0.10	0.24	-0.10	0.17	0.53	0.38
Beta Cal SD	0.11	0.13	0.09	0.09	0.04	0.14	0.19

Table 7. Mean intercalibration differences from each implementation for F13-F15

Method	19V	19H	22V	37V	37H	85/91V	85/91H
Polar Crossover	0.39	-1.10	0.16	-2.29	-2.56	1.77	0.00
Merra Simulation	0.92	-0.58	0.57	-1.83	-2.07	1.62	0.39
ERA-I Simulation	1.15	-0.52	1.05	-1.39	-1.70	1.82	0.69
TMI match (OE)	0.91	-0.60	0.58	-2.10	-2.43	1.66	0.68
TMI match (Merra)	0.95	-0.54	0.65	-2.09	-2.38	1.49	0.60
TMI match (ERA-I)	0.74	-0.75	0.47	-2.10	-2.41	1.64	0.61
VCC (OE)	0.25	-0.31	-0.33	-1.98	-0.94	0.99	1.31
VCC (Merra)	0.33	-0.86	-0.02	-2.08	-1.95	1.42	-0.51
VCC (ERA-I)	0.45	-0.96	-0.09	-2.18	-1.93	1.63	0.31
Mean Beta Mean	0.66	-0.75	0.35	-2.02	-2.11	1.61	0.38
Beta Cal SD	0.30	0.21	0.37	0.25	0.38	0.16	0.24

Table 8. Mean intercalibration differences from each implementation for F13-F16

Method	19V	19H	22V	37V	37H	85/91V	85/91H
Polar Crossover	0.41	-1.00	-0.30	-2.29	-1.69	3.78	2.49
Merra Simulation	0.26	-1.03	-0.47	-2.28	-1.75	3.68	2.69
ERA-I Simulation	0.42	-0.83	-0.06	-1.68	-1.36	3.72	2.87
TMI match (OE)	0.28	-1.12	-0.42	-2.50	-1.88	3.47	3.01
TMI match (Merra)	0.30	-1.08	-0.39	-2.50	-1.83	3.28	2.91
TMI match (ERA-I)	0.21	-1.13	-0.47	-2.47	-1.78	3.74	2.98
VCC (OE)	0.06	-0.04	-0.47	-2.61	-0.34	3.11	3.24
VCC (Merra)	-0.07	-0.95	-0.70	-2.68	-1.42	3.84	1.18
VCC (ERA-I)	-0.06	-1.07	-0.88	-2.77	-1.33	4.00	1.58
Mean Beta Mean	0.25	-0.93	-0.42	-2.36	-1.52	3.66	2.56
Beta Cal SD	0.16	0.15	0.16	0.26	0.30	0.10	0.37

Table 9. Mean intercalibration differences from each implementation for F13-F17

Method	19V	19H	22V	37V	37H	85/91V	85/91H
Polar Crossover	-	-	-	-	-	-	-
Merra Simulation	0.49	1.27	0.53	0.89	0.71	-0.58	-0.49
ERA-I Simulation	0.56	1.27	0.66	0.86	0.80	-0.44	-0.20
TMI match (OE)	0.72	1.59	0.73	1.04	1.13	-0.10	-0.09
TMI match (Merra)	0.72	1.59	0.72	1.05	1.15	-0.12	-0.11
TMI match (ERA-I)	0.60	1.52	0.65	1.03	1.05	-0.42	-0.14
VCC (OE)	0.06	0.29	-0.09	1.02	0.00	-1.02	-1.49
VCC (Merra)	0.41	1.18	0.47	1.18	0.95	-0.83	0.27
VCC (ERA-I)	0.36	1.23	0.55	1.14	1.06	-0.79	0.41
Mean Beta Mean	0.49	1.25	0.53	1.01	0.84	-0.53	-0.24
Beta Cal SD	0.17	0.27	0.16	0.10	0.19	0.27	0.10

Table 10. Mean intercalibration differences from each implementation for F17-F18

Appendix B: Plots of pairwise comparison summaries

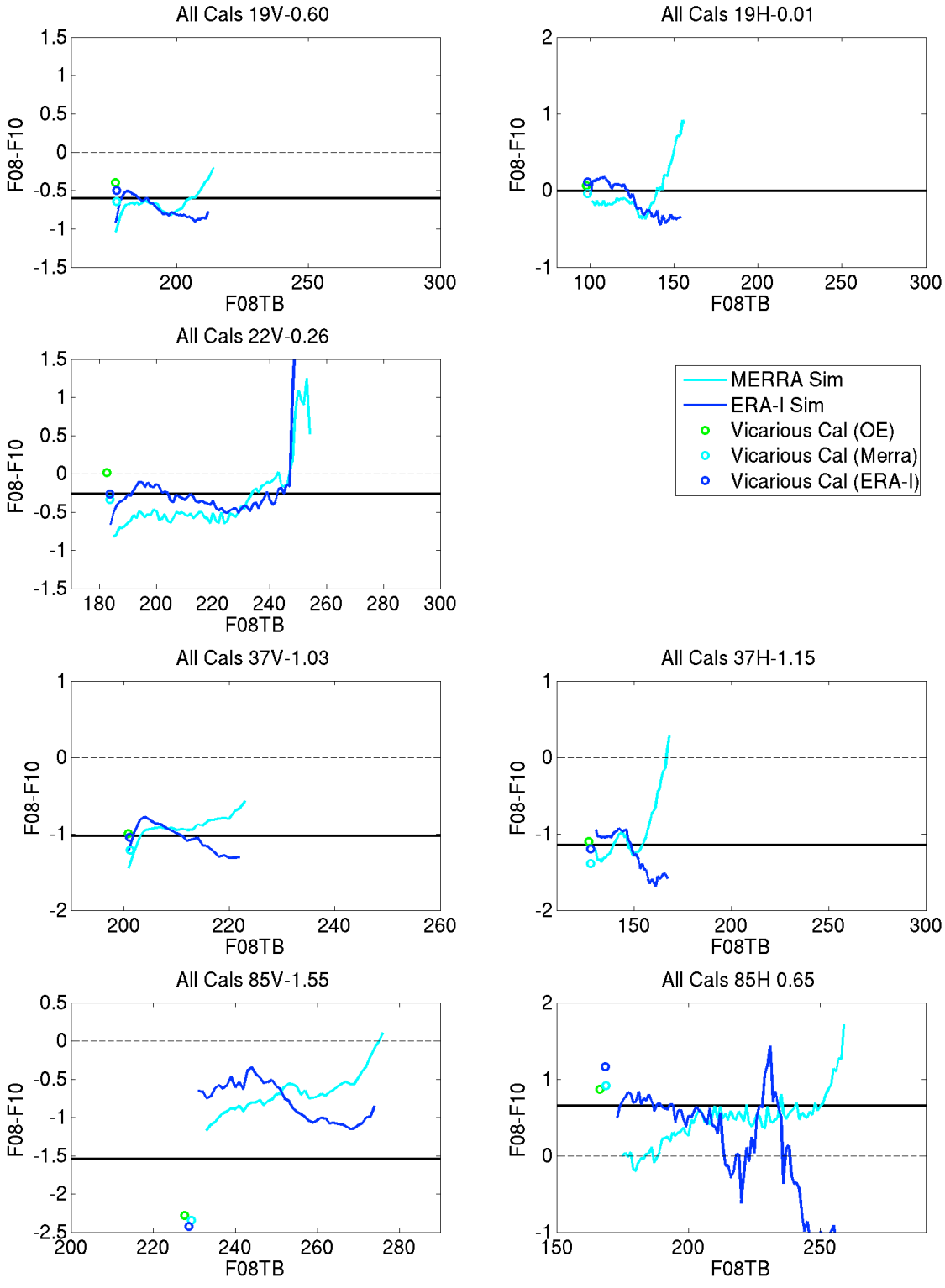

Figure B-1. Plots of intercalibration differences from each implementation by channel for F08-F10.

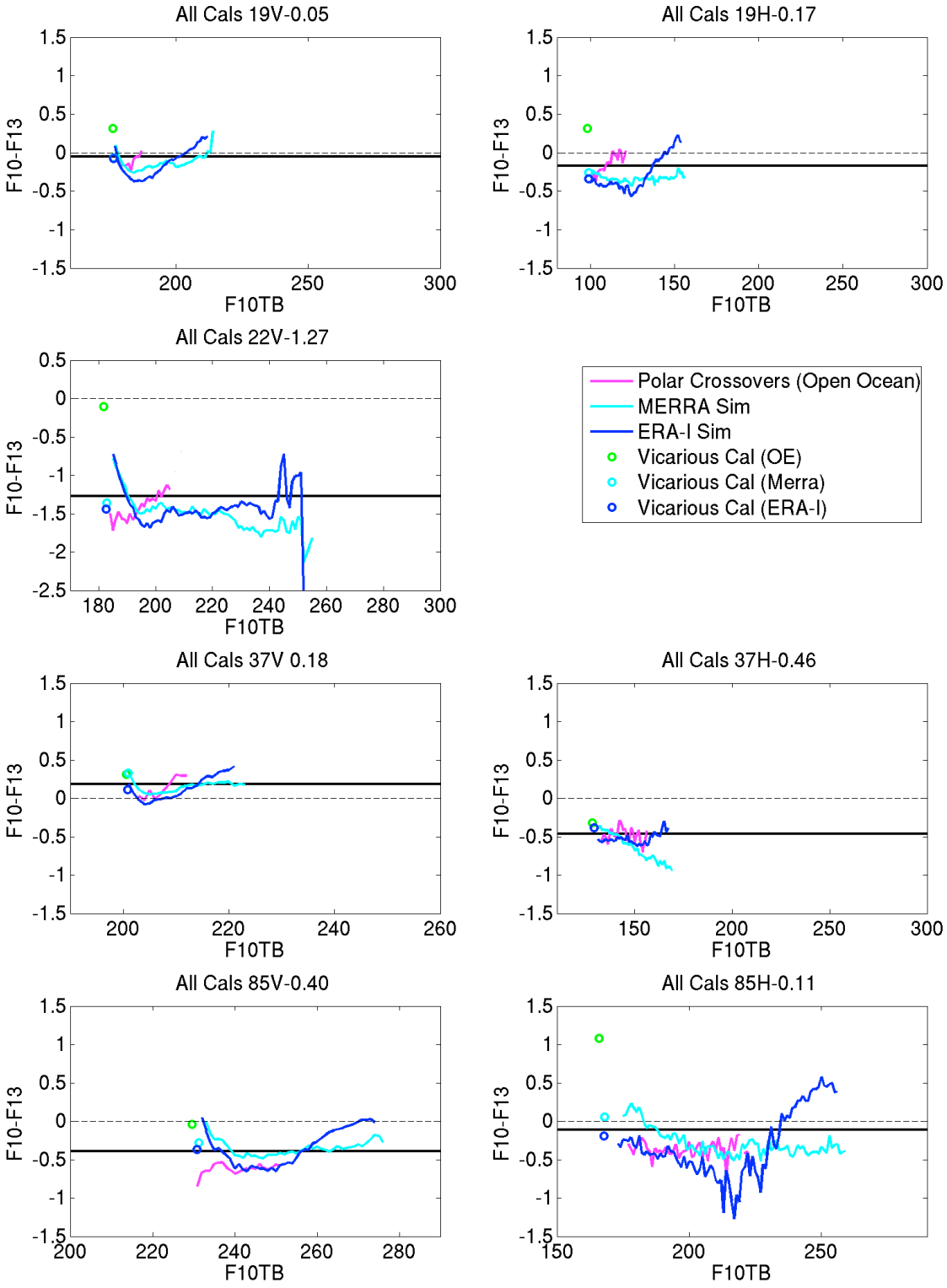

Figure B-2. Plots of intercalibration differences from each implementation by channel for F10-F13.

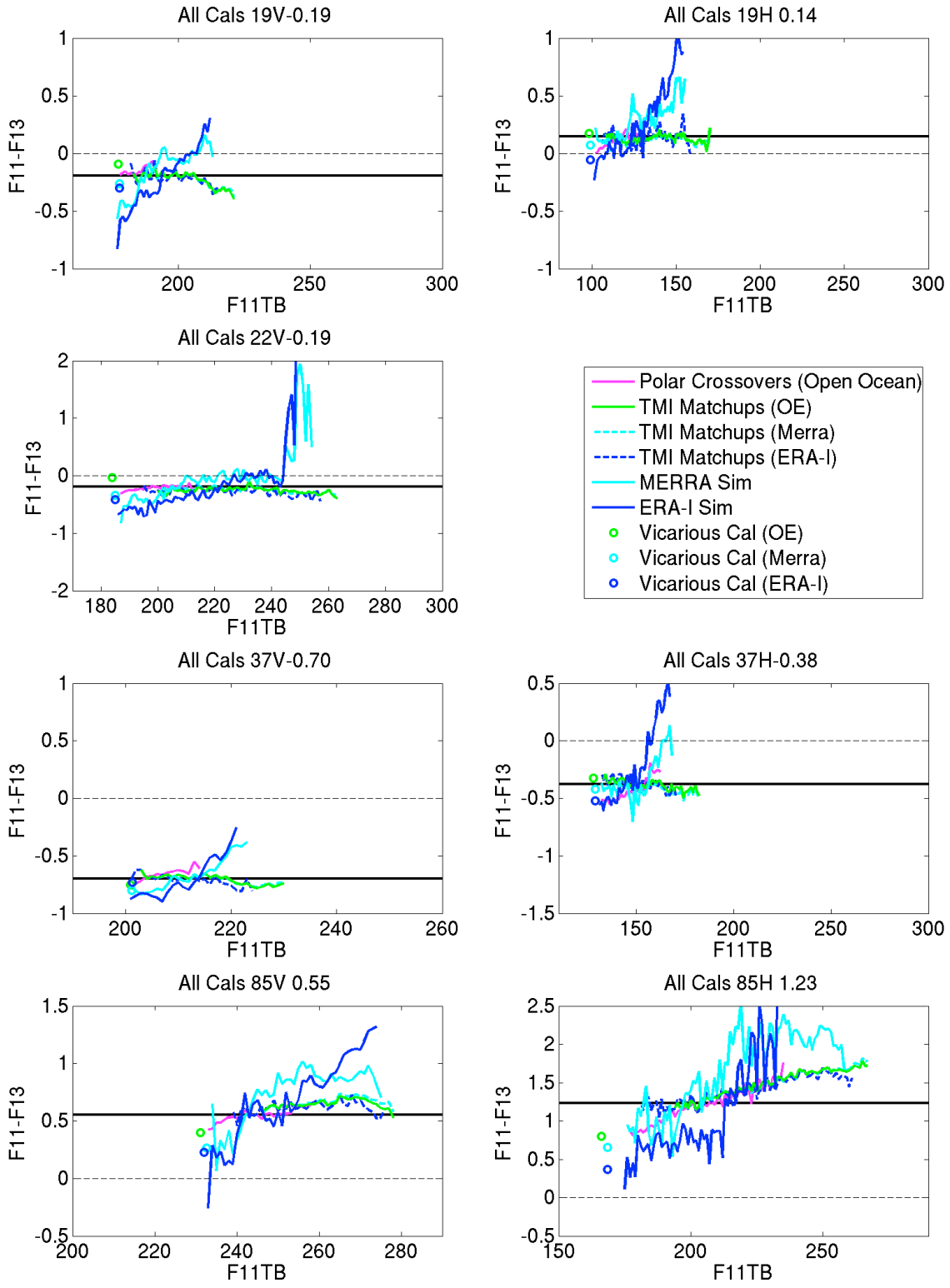

Figure B-3. Plots of intercalibration differences from each implementation by channel for F11-F13.

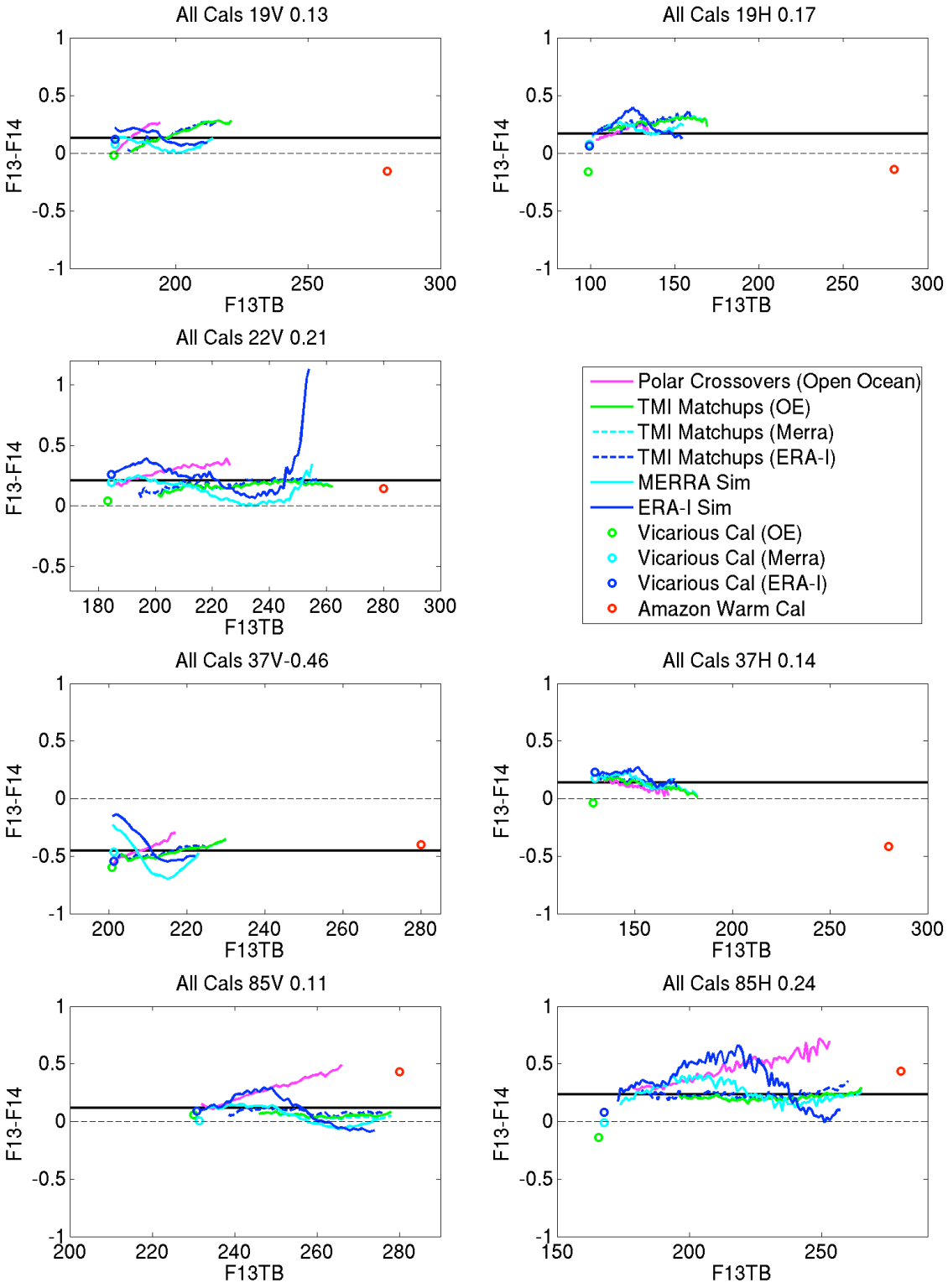

Figure B-4. Plots of intercalibration differences from each implementation by channel for F13-F14.

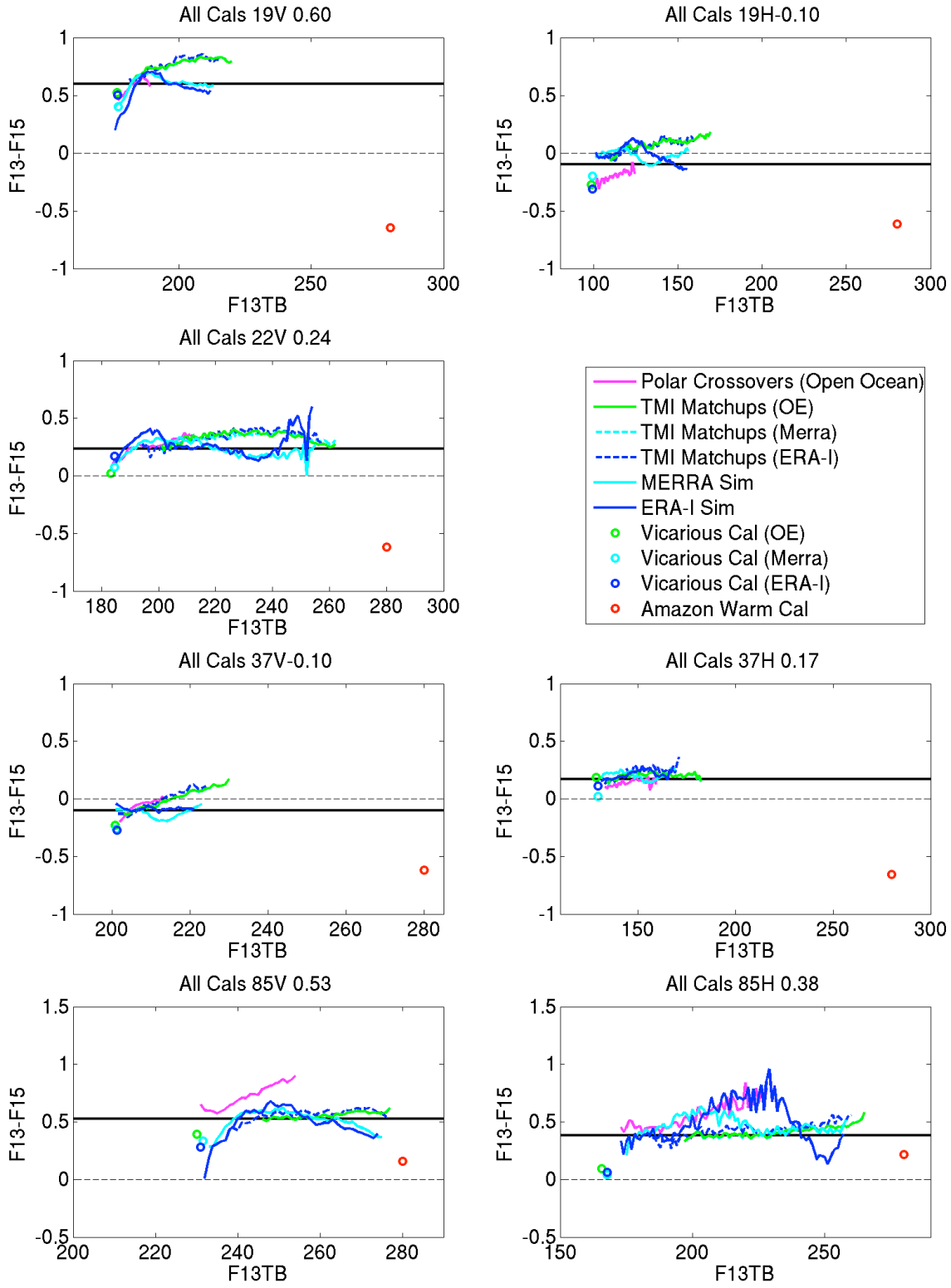

Figure B-5. Plots of intercalibration differences from each implementation by channel for F13-F15.

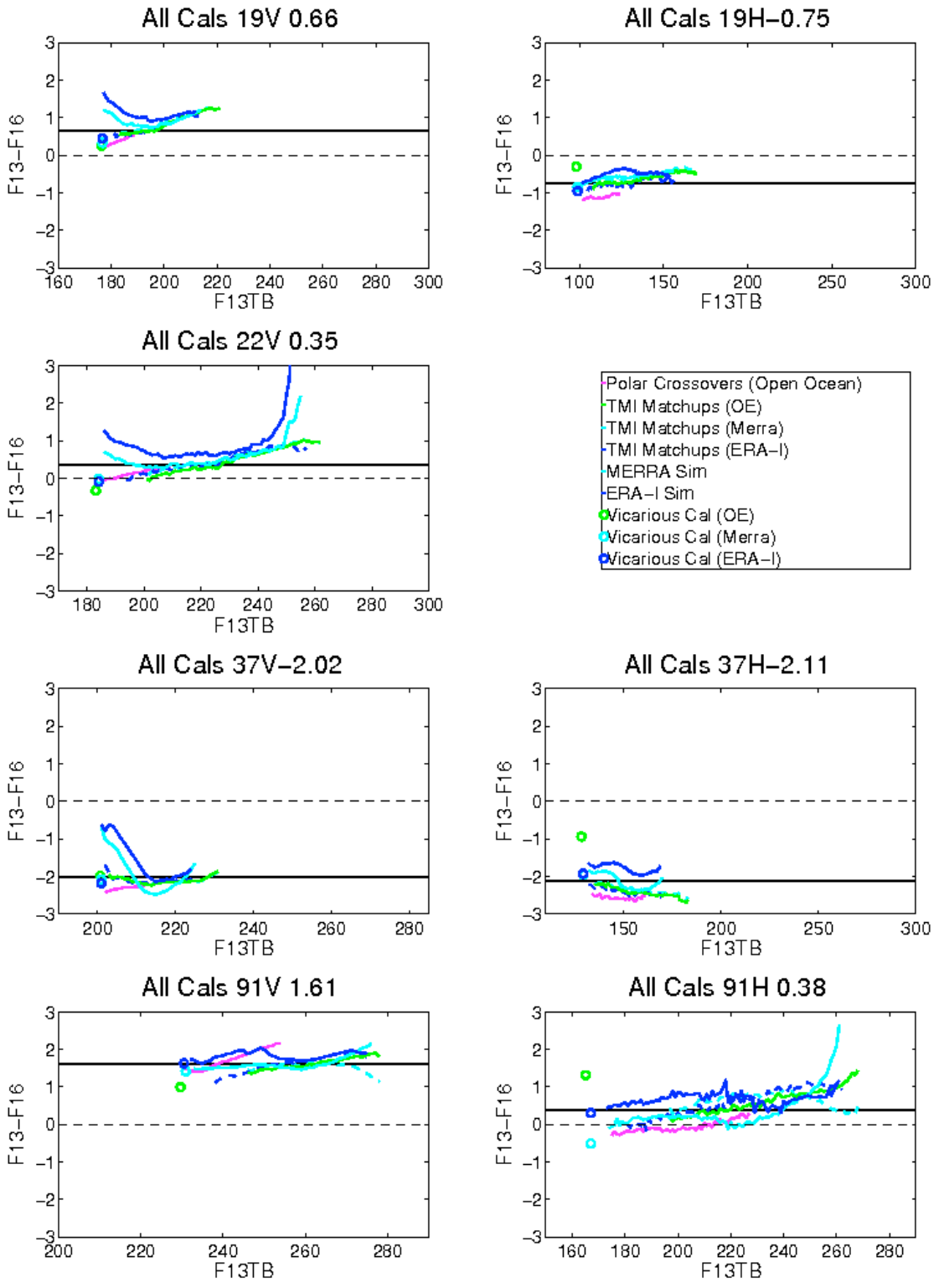

Figure B-6. Plots of intercalibration differences from each implementation by channel for F13-F16.

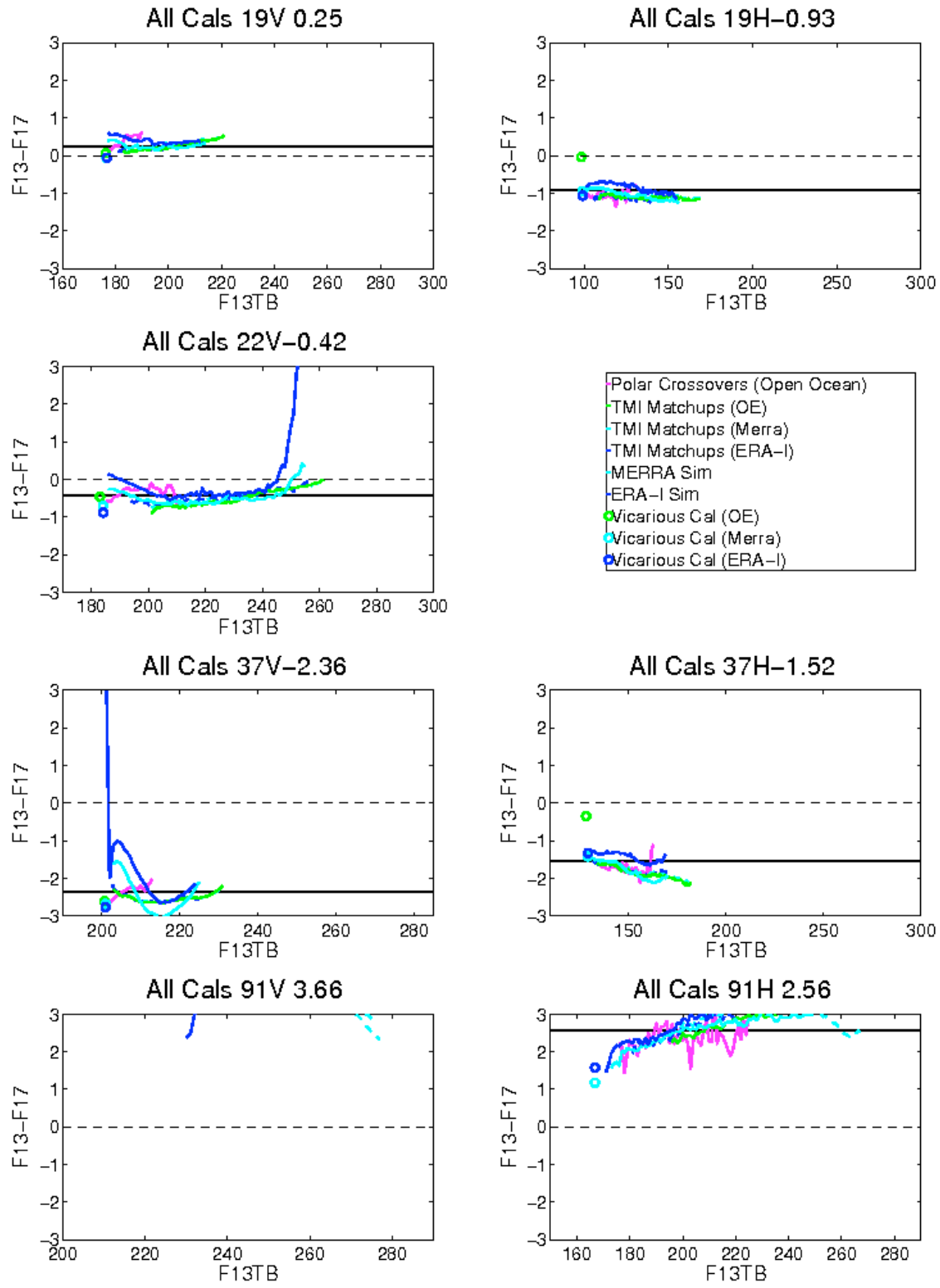

Figure B-7. Plots of intercalibration differences from each implementation by channel for F13-F17.

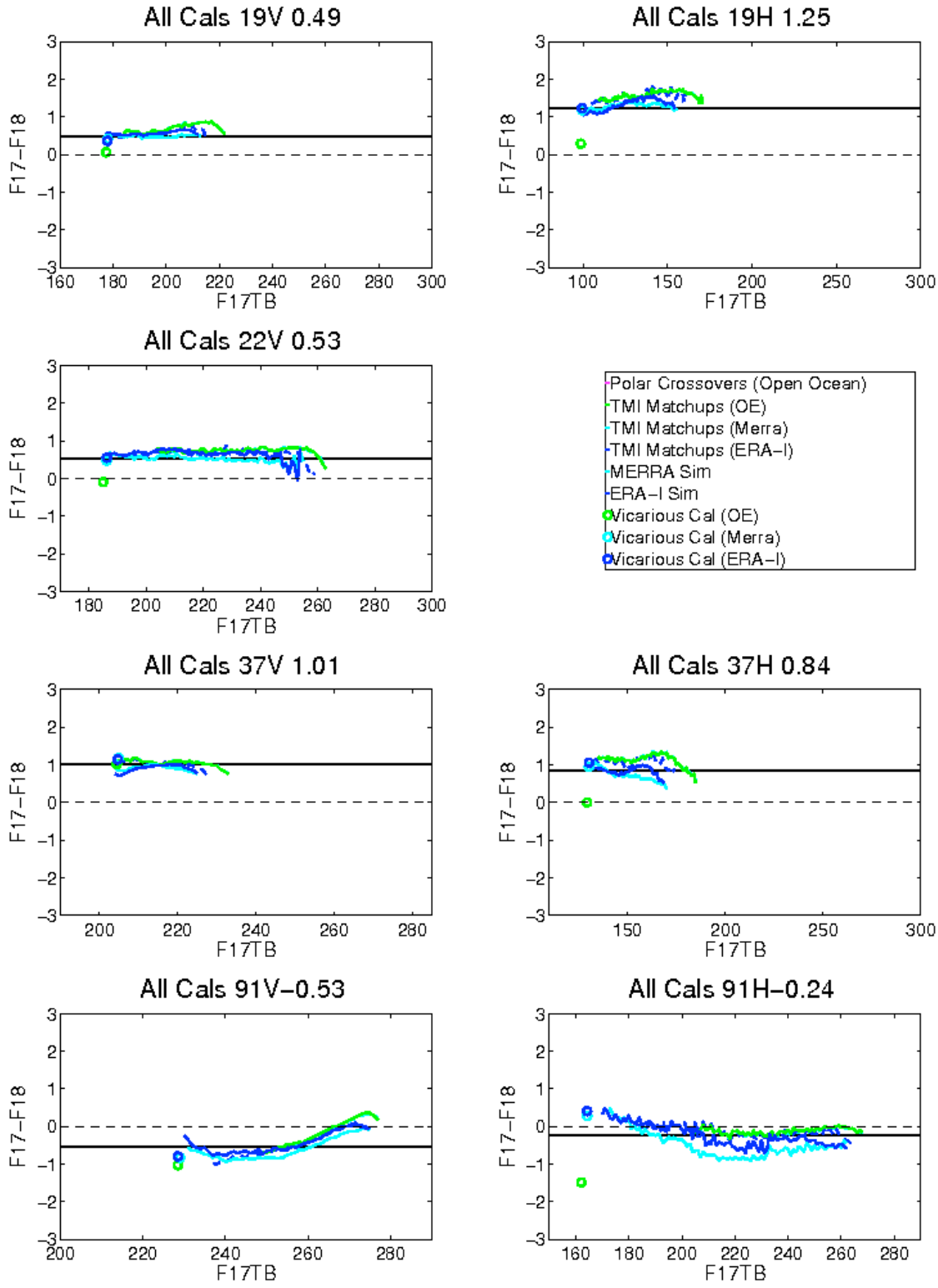

Figure B-8. Plots of intercalibration differences from each implementation by channel for F17-F18.